Back-arc extension in the Andaman Sea: tectonic and magmatic processes imaged by high-precision teleseismic double-difference earthquake relocation – Electronic Supplement

Diehl, T., Waldhauser, F., Cochran, J.R., Kamesh Raju, K.A., Seeber, L., Schaff, D. and Engdahl, E.R.

T. Diehl (Corresponding Author):
Lamont-Doherty Earth Observatory, Columbia University, Palisades, New York 10964, USA
Now at: Swiss Seismological Service, ETH Zurich, Sonneggstrasse 5, CH-8092, Zurich, Switzerland, Email: tobias.diehl@sed.ethz.ch, Phone: +41 44-632-0498

F. Waldhauser, J.R. Cochran, L. Seeber, D. Schaff:
Lamont-Doherty Earth Observatory, Columbia University, Palisades, New York 10964, USA

K.A. Kamesh Raju:
National Institute of Oceanography, Dona Paula, Goa 403 004, India

E.R. Engdahl:
Department of Physics, University of Colorado, Boulder, Colorado 80309, USA

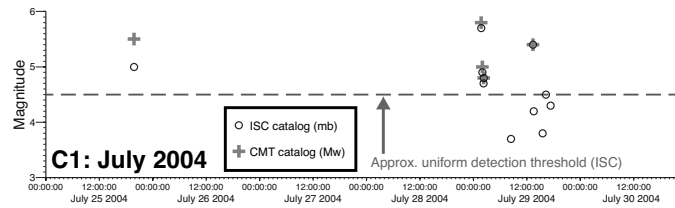## S.1 Characteristics of earthquake sequences in the Andaman Sea

Figure S1 describes the overall temporal clustering of seismicity in the back-arc region between 1964 and 2009. Figures S2-S4 illustrate the characteristics of different earthquake sequences in the back-arc region in terms of event time and magnitude.
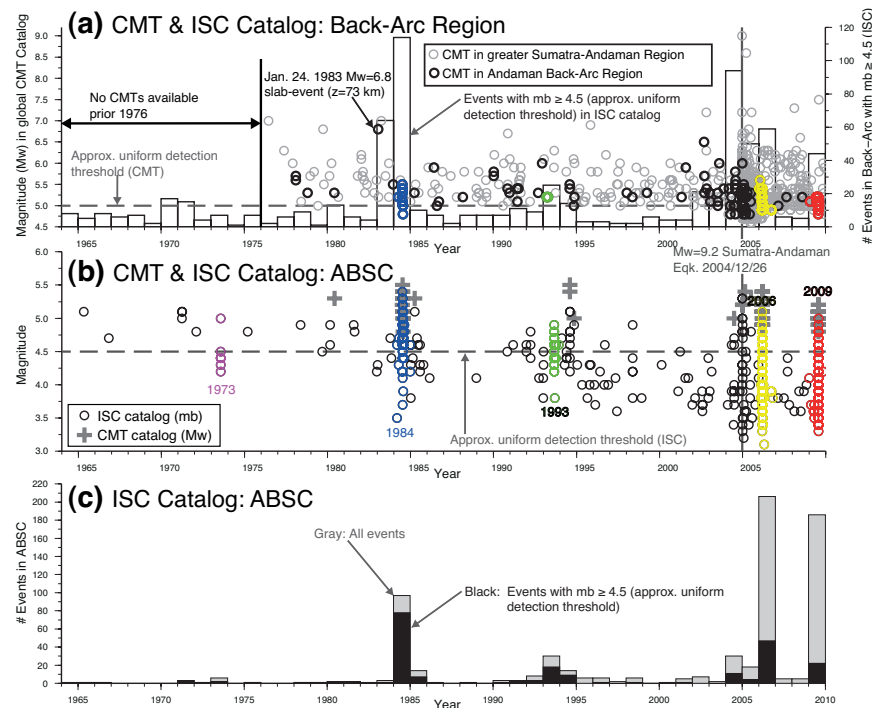

Figure S1. Seismicity in the Andaman Sea back-arc region between 1964 and 2009. (a) Thin gray circles indicate Mw in the greater Sumatra-Andaman region (area shown in Figure 1) as reported in the global CMT catalog. Bold circles indicate Mw in the back-arc region as reported in the global CMT catalog. Histogram in the background indicates number of events per year (with mb ≥ 4.5) in the back-arc region as reported in the ISC catalog. (b) Circles indicate mb for earthquakes within the Andaman Back-Arc Spreading Center (ABSC) as reported in the ISC catalog. Crosses indicate Mw for earthquakes within the ABSC as reported in the global CMT catalog. (c) Number of events per year in the ABSC as reported in the ISC catalog. Gray indicates all events in the ABSC. To account for a uniform detection threshold, black bars indicates number of events with mb ≥ 4.5.
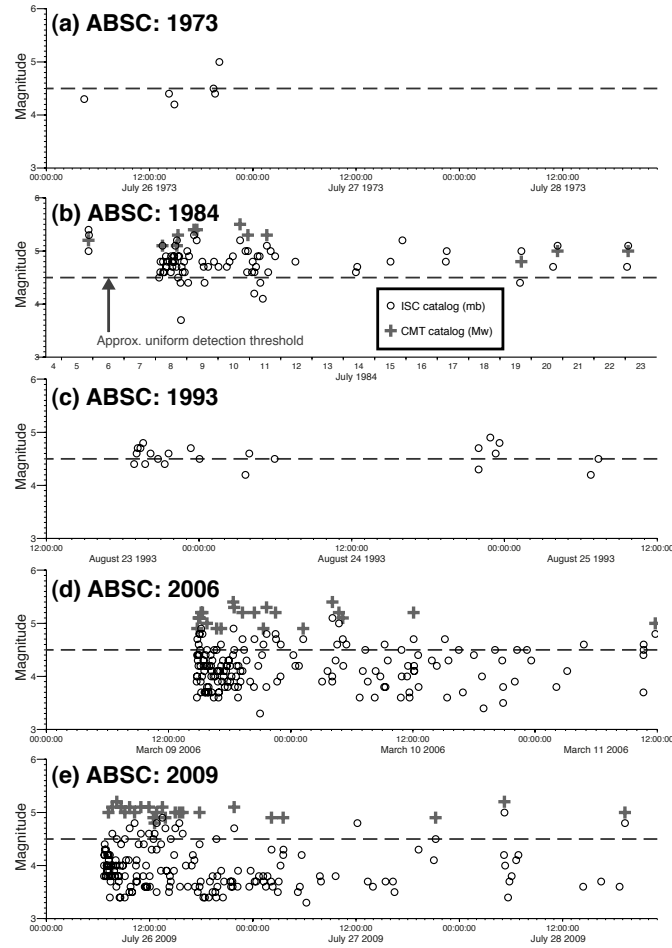
Figure S2. Characteristics of earthquake sequences in the ABSC in terms of event time and magnitude. Circles indicate mb as reported in the ISC catalog. Crosses indicate Mw as reported in the global CMT catalog. Typical for swarm-like sequences, the largest magnitudes occur in the middle of the sequences and magnitudes do not decay as observed in typical mainshock-aftershock sequences.

Figure S3. Characteristics of an earthquake sequence in the northeastern part of the back-arc region (cluster C1 in Figure 4b and 5) in terms of event time and magnitude. Circles indicate mb as reported in the ISC catalog. Crosses indicate Mw as reported in the global CMT catalog. A precursor-event on July 25 is followed by the main-shock on July 29. 2004. In contrast to the swarms in the ABSC, magnitudes rapidly decrease after the mainshock, suggesting a typical mainshock-aftershock behavior of this sequence.
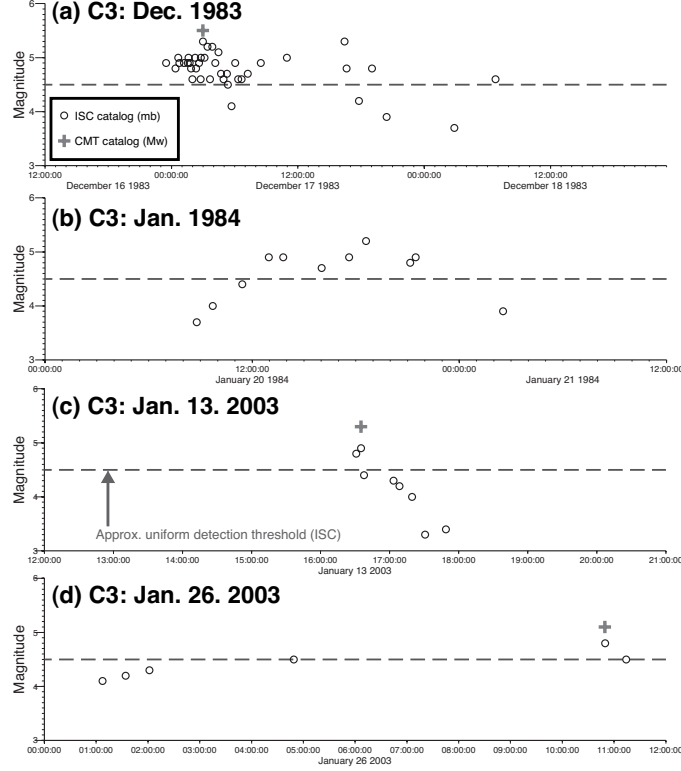
Figure S4. Characteristics of earthquake sequences in the northeastern part of the back-arc region (cluster C3 in Figure 4d and 5) in terms of event time and magnitude. Circles indicate mb as reported in the ISC catalog. Crosses indicate Mw as reported in the global CMT catalog. Sequences in a, b, d show typical swarm-like characteristics, whereas the sequence in c indicates a mainshock-aftershock behavior.

S.2 Assessment of absolute location robustness

Accuracy in absolute locations is crucial for interpretation of underlying mechanisms, especially if seismicity is correlated with surface structures (e.g. seafloor morphology). The absolute position of DD-solutions strongly depends on the accuracy of the initial hypocenters. Since the EHB locations are the reference base for the overall absolute location of the DD solutions, possible bias in the EHB locations would also affect the absolute position of the DD-solutions. Such bias may result from deviations of the true structure from the 1D velocity model ak135 used to locate the events (presence of slab, etc.) and bias in station geometry.

To assess the effect of source-side 3D velocity structure on the location of earthquakes in the Andaman Sea, we calculated theoretical *P*-wave travel times (first arriving phases only; distances ≤95º) in a 3D velocity model [*Widiyantoro and van der Hilst*, 1997] for a series of synthetic hypocenters (black dots in Figure S5). A synthetic, symmetrical distribution of receivers (gray triangles in Figure S5) is chosen to eliminate effects due to station geometry. A grid-search, using a global 1D model (ak135), is performed around the true hypocenter, with a resolution of 1 km in latitude and longitude and 0.1 s in origin time. The focal depth is fixed to 10 km, though tests with floating focal depths show only biases in origin time. Gray arrows in Figure S5 indicate direction and amplitude of epicenter-mislocations due to the effect of unmodeled source-side 3D velocity structure.

In general, solutions in the 1D model tend to locate north of their 3D location with a mean mislocation of about 5 km.

To assess the additional effect of the network geometry, travel times are calculated for the same set of sources in the 3D model, using a realistic station distribution (black triangles in Figure S5) taken from an earthquake in the Andaman Spreading Center (mb=5.1). Only stations reporting P phase picks in the ISC bulletin are considered. The combined effect of 3D structure and network geometry is shown in Figure S5 by black arrows. Along the central and the eastern segment of the spreading center, the effect of network geometry compensates the mislocation caused by unmodeled 3D structure, and the net mislocation is smaller than 1 km. Mean shift in origin time is on the order of -1 s in both tests. Systematic errors in absolute location caused by the combined effect of unmodeled 3D velocity structure and potential bias due to heterogeneous station distribution are less than 1 km in longitude and less than 5 km in latitude for most parts of the Andaman Sea. EHB epicenters might be located slightly south of their true location.

Effects of the 3D velocity structure on the absolute focal depths were not explicitly studied in this test. The absolute depths of the initial locations strongly depend on depth phases. Relative depths, however, are reasonably well constrained because of the differential core phases with their steep takeoff angles. Insufficient linkage of depth and core phases can result in poorly constrained focal depth of individual earthquakes.
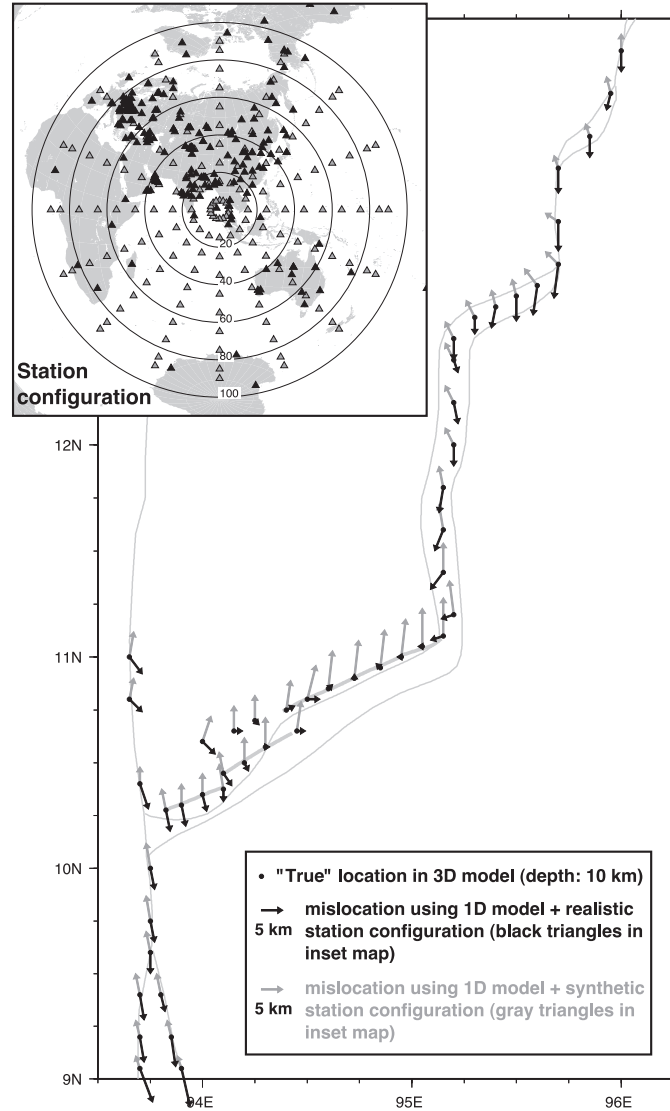
Figure S5. Arrows indicate direction and amplitude of absolute mislocation of epicenters (in kilometers) caused by using a global 1D velocity model (ak135). Gray arrows correspond to a synthetic station configuration (gray triangles in inset map), reflecting pure model effects. Black arrows correspond to a realistic station configuration (black triangles in inset map), reflecting combined effect of 3D structure and network geometry. Position of synthetic hypocenters is indicated by black dots. Tectonic features (after *Curray* [2005]) are indicated by thin gray lines, ridge segments as defined by *Kamesh Raju et al.* [2004] are indicated by bold gray lines. Circles in inset map correspond to great-circle distances in degree.

S.3 b-value analysis

The frequency-magnitude distribution describes the relationship between the frequency of occurrence and the magnitude of earthquakes. The b-value describes the relative size distribution of events and can be indicative of the material's heterogeneity, increase in pore pressure, or the stress regime [e.g., Mogi, 1962; Wiemer et al., 1998; Schorlemer et al., 2005]. To see if differences in the frequency-magnitude distribution exist, we calculated b-values for different parts of the back-arc region by using a maximum-likelihood technique [e.g. *Aki*, 1965; *Bender*, 1983; *Woessner and Wiemer*, 2005]. The magnitude of completeness (*Mc*) was determined visually by assessing the cumulative sum as well as the absolute number of magnitudes in the magnitude bins. Due to the narrow range in magnitudes and the relatively small number of events, the derived b-

5

values likely have large uncertanties and should only be considered "suggestive". The results are very sensitive to Mc, which is difficult to determine in case of such narrow range in magnitude and the small number of events. Figure S6 shows individual b-values for the three major swarms in the ABSC derived from mb as reported in the ISC catalog. Figure S7 shows b-values for three different sub-regions in the back-arc derived from mb in the ISC catalog and Mw in the global CMT catalog. Our results suggest that b-values in the ABSC appear to be higher than anywhere else in the back-arc region. As for other volcanic regions in the world, the high b-values might be indicative for active volcanic processes in the ABSC.
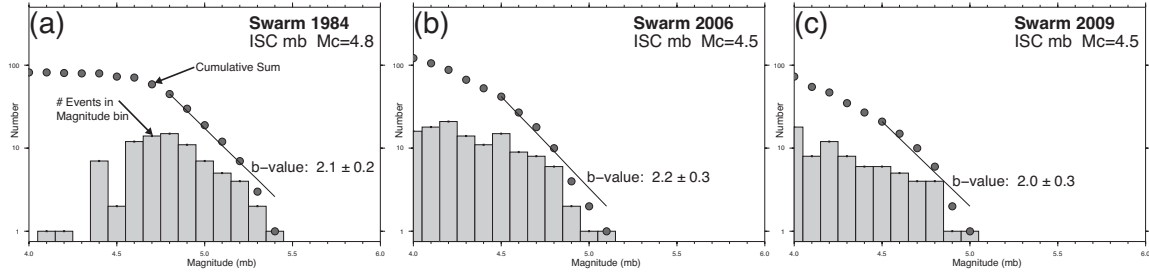
Figure S6. b-values for three major swarms in the ABSC derived from mb as reported in the ISC catalog. Dots indicate cumulative sum of magnitude readings, histograms indicate absolute number of magnitude reading per magnitude bin.
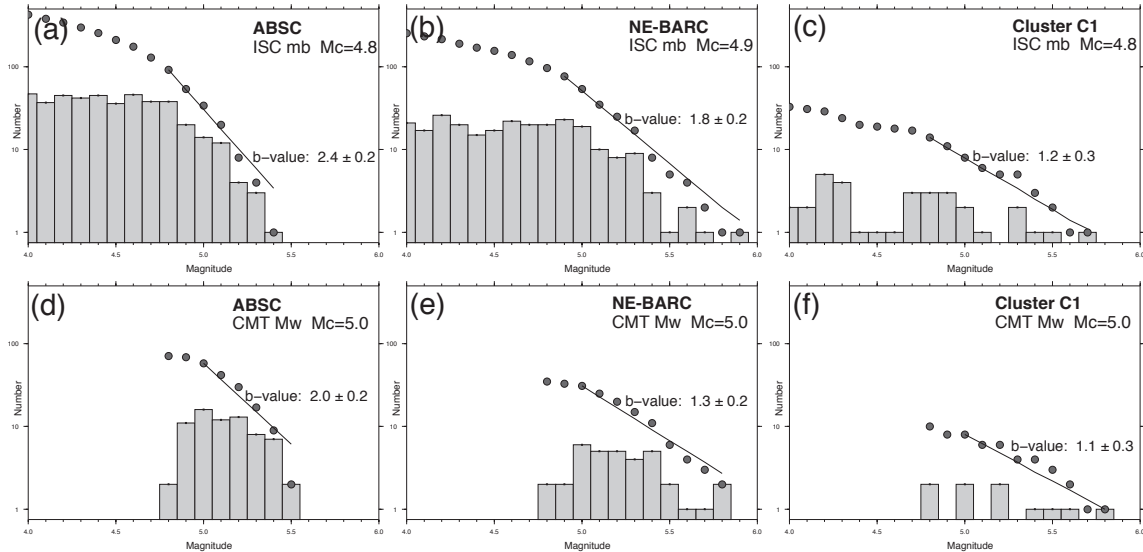
Figure S7. b-values for three different sub-regions in the back-arc derived from mb in the ISC catalog (a-c) and Mw in the global CMT catalog (d-f). Dots indicate cumulative sum of magnitude readings, histograms indicate absolute number of magnitude reading per magnitude bin. b-values in the ABSC appear higher than elsewhere in the back-arc region.

S.4 CLVD analysis of global CMT solutions

The non-double-couple part of the moment tensor is described by the compensated-linear-vector-dipole (CLVD) component [*Knopoff and Randall*, 1970; *Frohlich*, 1990]. Special types of non-double-couple mechanisms are vertical-CLVD earthquakes, which have large non-double-couple component and steeply plunging P- or T-axis. Such vertical-CLVD earthquakes often correlate in space and time with episodes of volcanic unrest and are interpreted to be the result of volcanic processes [e.g., *Ekström*, 1994;

Nettles and Ekström, 1998; *Shuler et al.*, 2013]. One of the physical models proposed for such vertical-CLVD mechanisms suggests dip-slip motion on volcano ring faults [*Ekström*, 1994].

To see whether or not such vertical-CLVD mechanisms exist in the back-arc region we analyzed moment tensor solutions in the global CMT catalog following the approach of *Shuler et al.* [2013]. The non-double-couple component is defined as

$$\varepsilon = -\lambda_2 / \max(|\lambda_1|, |\lambda_3|),$$

where λ_1 is the largest eigenvalue, λ_3 is the smallest eigenvalue, and λ_2 is the intermediate eigenvalue of the moment tensor. Pure double-couple earthquakes have $\varepsilon=0$ and pure CLVD mechanisms have $\varepsilon=\pm0.5$. Following *Shuler et al.* [2013] we calculated ε for all moment tensors in the global CMT catalog, which are within the back-arc region. We found 24 solutions with $|\varepsilon| > 0.2$, which are shown in Figure S8. Only 3 of those events are located within the ABSC region. Using the definition for vertical-P CLVD events ($\varepsilon < -0.2$, plunge of P-axis $>60°$) of *Shuler et al.* [2013] we found three of such events in the back-arc region (vPC1-vPC3 in Figure S8). Only one of them (vPC1) is located within the ABSC and part of the 1984 swarm. In addition, we found one vertical-T CLVD event ($\varepsilon > +0.2$, plunge of T-axis $>60°$) in the back-arc region (vTC1 in Figure S8), which is probably related to the plate interface. *Shuler et al.* [2013] pointed out that adding additional mantle-wave and surface-wave data can significantly reduces the size of the CLVD component of the CMT solution. Therefore we cannot rule out the possibility that some of the events shown in Figure S8 are in fact close to double-couple mechanisms.
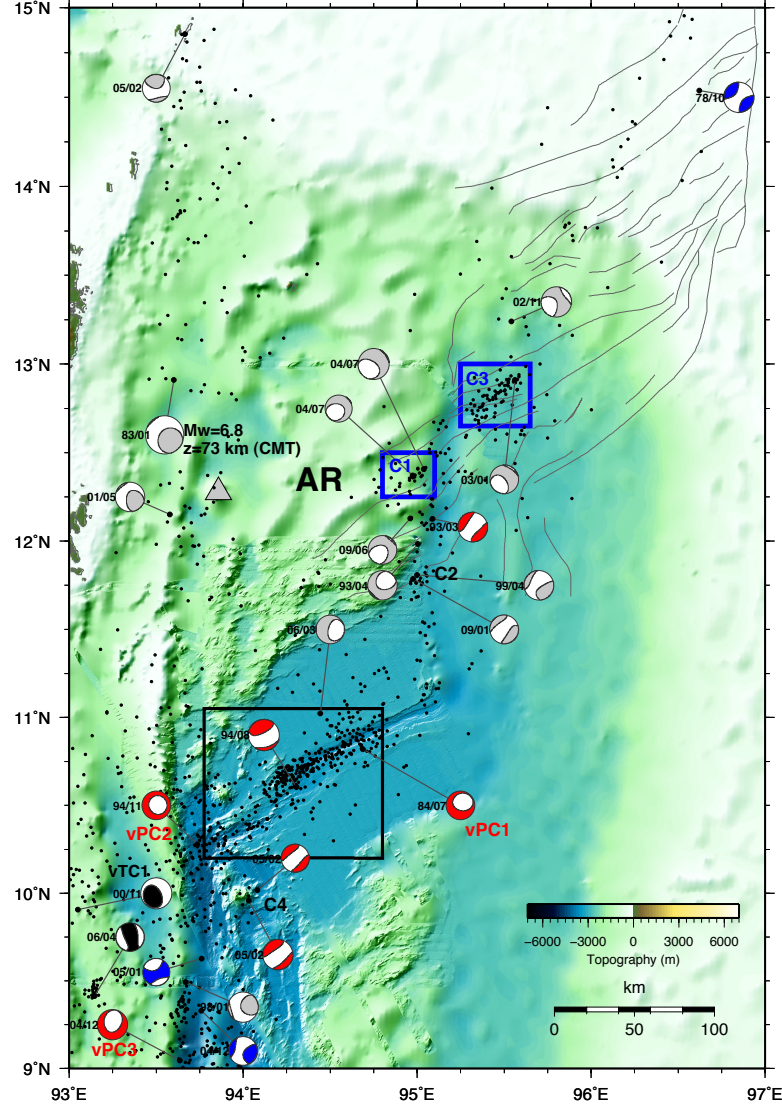
Figure S8. CMT solutions with significant non-double-couple components (|ε| > 0.2) in the back-arc region. Label left of beach-ball symbols denotes year/month of event. Mechanisms labeled vPC1-vPC3 fall in the category of vertical-P CLVD earthquakes, mechanism labeled vTC1 falls in the category of a vertical-T CLVD earthquake.

S.5 Regional gravity and magnetic anomalies

In Figure S9 we overlay regional free-air gravity [*Sandwell and Smith*, 2009] and magnetic anomalies [*Maus et al.*, 2009] with the relocated seismicity of this study. The north-south striking negative anomaly in the gravity data in-between the Andaman Islands and the WAF (Figure S9a) was previously interpreted by *Curray* [2005] as indication for low-density sediments in the accretionary complex. The positive anomaly around 93.5°E/11.25°N, on the other hand, was interpreted as uplifted volcanics and/or intrusives [*Curray*, 2005]. The magnetic data in Figure S9b features an area of high magnetization over the ABSC, which probably reflects the presence of younger, highly magnetic crust in that region.
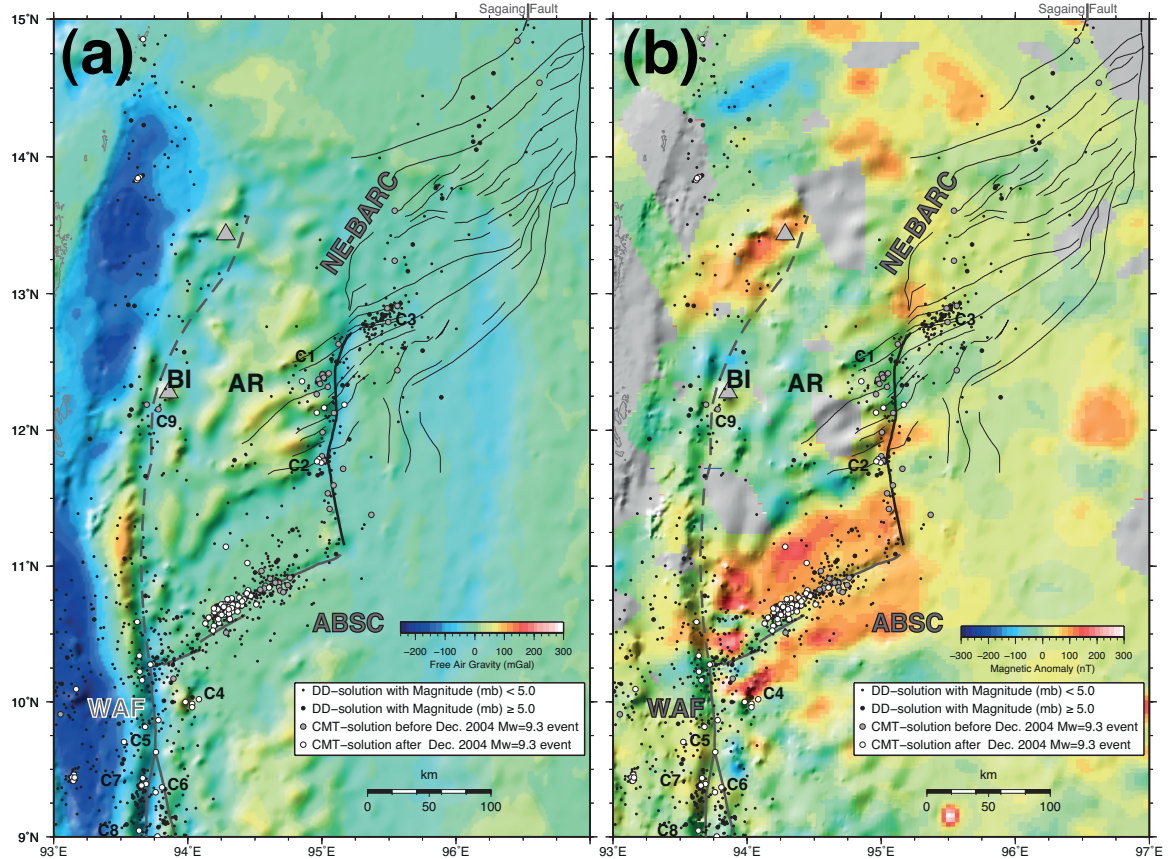
Figure S9. (a) Satellite-derived free-air gravity anomalies [*Sandwell and Smith*, 2009], draped over bathymetric relief. Dots indicate relocated seismicity in the back-arc region. White and gray dots indicate events with CMT solutions. (b) Magnetic anomaly data (EMAG2 V2, Maus et al. [2009]) draped over bathymetric relief.

S.6 Coulomb stress change modeling

In order to compare the amplitudes of the post-2004 regional stress change (in the order of 0.2-0.3 bar) to local stresses resulting from a dike intrusion, we modeled the Coulomb stress change due to a hypothetical tensile opening at the location of the 2006 earthquake swarm. We used two different receiver fault geometries based on the CMT solutions displayed in Figure 10:

- Steeply dipping axial faults (average for axial events):

strike=73°, dip=58°, rake=-92°

- Moderately dipping off-axis faults (average for events in fault-scarp region):

strike=63°, dip=36°, rake=-96°

The finding of the modeling is that local stress changes due to a hypothetical intrusion significantly exceed possible coseismic stress perturbations that may have originated from the Dec. 2004 rupture. The difference in stress change is in the order of one magnitude and this finding is rather independent from the parameters used in the modeling as shown by Figure S10. Figure S10a shows the Coulomb stress change at 1 km depth using the parameters described in section 4.3 of the paper:

- Tensile opening of 1 m: Typical values found in literature.

- Dike height: 1.5 km (from 5.5 km to 4 km depth): Typical values found in literature.

- Along-strike length of dike 37 km: Based on extent of axial seismicity in the first 4

9

hours of the 2006 swarm.

Most axial events are included within the 5 bar isoline. Parameters used in Figure S10b are identical to S10a, except that the dike height was reduced to 1 km (from 5.5 km to 4.5 km depth). Most axial events are located within the 1-2 bar isoline. In Figure S10c the along-strike length of the dike was reduced to 33 km and in Figure S10d the tensile opening was reduced to 0.5 m. In both cases, the majority of the axial events are located within the 1-2 bar isoline. In all models, axial events are located within the 1-2 bar isoline and stress change amplitudes significantly exceed the 0.2-0.3 bar predicted by coseismic stress models for the Dec. 2004 rupture. Perturbations in the modeled dike geometry mainly affect the stress change amplitudes in the off-axis regions.
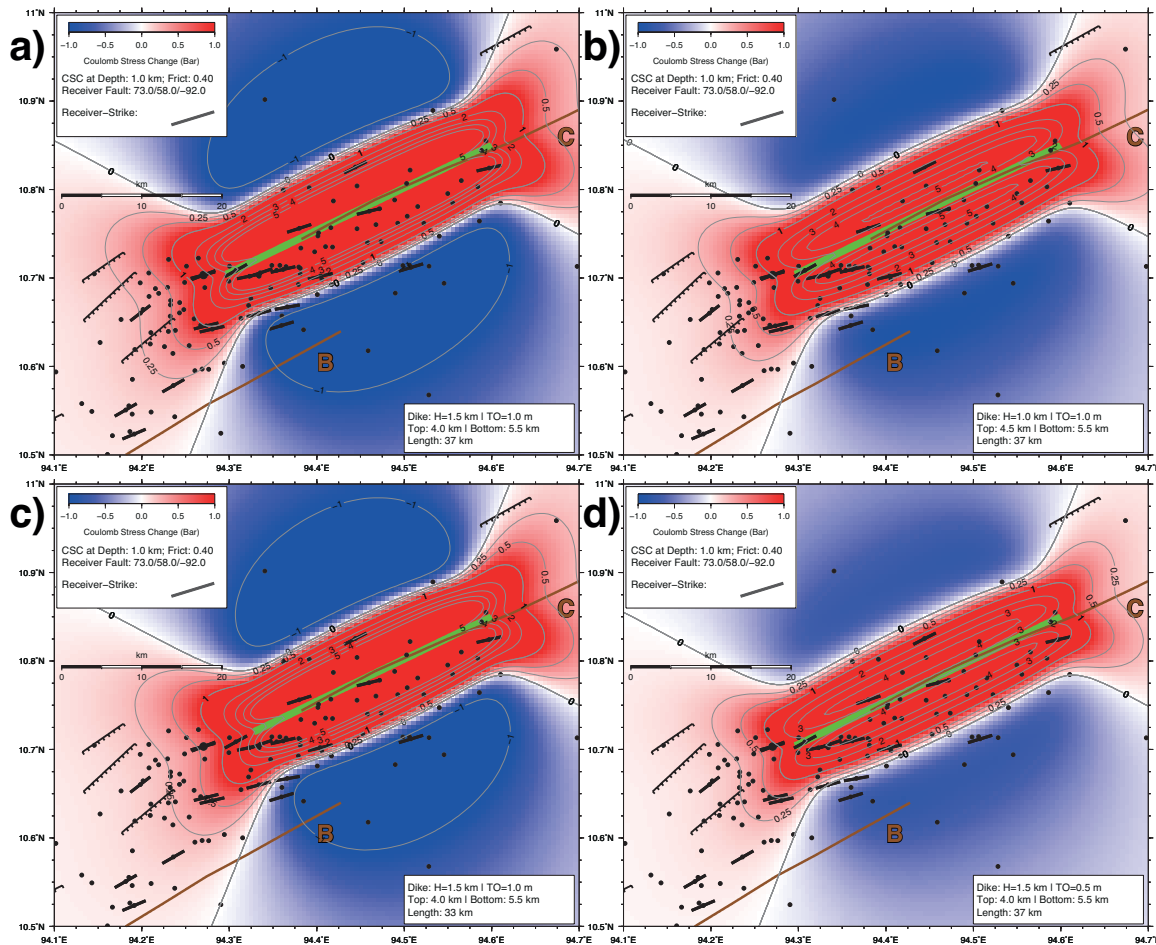
Figure S10. Results of the Coulomb stress modeling for different dike geometries along segment C of the ABSC. The green line indicates the along strike extent of the hypothetical dike, black dots indicate epicenters of the 2006 earthquake swarm, black bars indicate direction of CMT B-axes. Faults identified from high-resolution bathymetric data are shown by black. (a) Dike geometry described in section 4.3 of the paper. (b) Dike height reduced to 1 km. (c) Along-strike extent reduced to 33 km. (d) Tensile opening reduced to 0.5 m.

References (Electronic Supplement)

Aki, K. (1965), Maximum likelihood estimate of b in the formula log N = a-bM and its confidence limits, *Bull. Earthq. Res. Inst. Tokyo Univ., 43*, 237–239.

Bender, B. (1983). Maximum likelihood estimation of b-values for magnitude grouped data, *Bull. Seism. Soc. Am., 73*, 831–851.

Curray, J. R. (2005), Tectonics and history of the Andaman Sea region, *J. Asian Earth Sci., 25*(1), 187-228.

Ekström, G. (1994), Anomalous earthquakes on volcano ring-fault structures, *Earth Planet. Sci. Lett., 128*, 707–712.

Frohlich, C. (1990), Earthquakes with non-double-couple mechanisms, *Science, 264*, 804–809.

Kamesh Raju, K. A., T. Ramprasad, P. S. Rao, B. R. Rao, and J. Varghese (2004), New insights into the tectonic evolution of the Andaman basin, northeast Indian Ocean, *Earth Planet Sci. Lett., 221*(1-4), 145-162.

Knopoff, L., and M. J. Randall (1970), The compensated linear-vector dipole: A possible mechanism for deep earthquakes, *J. Geophys. Res., 75*(26), 4957–4963.

Maus, S. et al. (2009), EMAG2: A 2-arc min resolution Earth magnetic anomaly grid compiled from satellite, airborne, and marine magnetic measurements, *Geochem. Geophys. Geosyst., 10*(Q08005), doi:10.1029/2009GC002471.

Mogi, K. (1962), Magnitude-frequency relations for elastic shocks accompanying fractures of various materials and some related problems in earthquakes, *Bull. Earthq. Res. Inst. Tokyo Univ., 40*, 831-853.

Nettles, M., and G. Ekström (1998), Faulting mechanism of anomalous earthquakes near Bárdarbunga Volcano, Iceland, *J. Geophys. Res., 103*(B8), 17,973–17,983.

Sandwell, D., and W. Smith (2009), Global marine gravity from retracked Geosat and ERS-1 altimetry: ridge segmentation versus spreading rate, *J. geophys. Res., 114*(B01411), doi:10.1029/2008JB006008.

Schorlemmer, D., S. Wiemer, and M. Wyss (2005), Variations in earthquake-size distribution across different stress regimes, *Nature, 437*, 539-542.

Shuler, A., M. Nettles, and G. Ekström (2013), Global observation of vertical-CLVD earthquakes at active volcanoes, *J. Geophys. Res. Solid Earth*, *118*, doi:10.1029/2012JB009721.

Widiyantoro, S., and R. van der Hilst (1997), Mantle structure beneath Indonesia inferred from high-resolution tomographic imaging, *Geophys. J. Int.*, *130*(1), 167-182.

Wiemer, S., S. McNutt, and M. Wyss (1998), Temporal and threedimensional spatial analyses of the frequency-magnitude distribution near Long Valley Caldera, California, *Geophys. J. Int.*, *134*, 409–421, doi:10.1046/j.1365-246x.1998.00561.x.

Woessner, J. and S. Wiemer (2005), Assessing the quality of earthquake catalogues: estimating the magnitude of completeness and its uncertainty, *Bull. Seism. Soc. Am., 95*, 684–698.